Acta Astronautica 211 (2023) 333–343

Contents lists available at ScienceDirect

Acta Astronautica

journal homepage: www.elsevier.com/locate/actaastro

Selected results of the hypersonic flight experiment STORT

A. Gülhan [a,*], D. Hargarten [b], M. Zurkaulen [b], F. Klingenberg [a], F. Siebe [a], S. Willems [a], G. Di Martino [c], T. Reimer [c]

[a] Supersonic and Hypersonic Technologies Department, Institute of Aerodynamics and Flow Technology, German Aerospace Center (DLR), Cologne, Germany
[b] Mobile Rocket Base (MORABA) Department, Institute of Space Operations and Astronaut Training, German Aerospace Center (DLR), Oberpfaffenhofen, Germany
[c] System Integration Department, Institute of Structures and Design, German Aerospace Center (DLR, Stuttgart, Germany

ARTICLE INFO

Keywords:
STORT
Sounding rocket
Flight experiment
Hypersonic
Thermal management

ABSTRACT

The three-stage rocket configuration of the hypersonic experiment STORT with several scientific payloads concerning hypersonic technologies was launched successfully from the Andøya Space launch site in northern Norway on June 26, 2022. The third stage performed a suppressed trajectory to increase integral heat load on the payload structures. The vehicle traveled at speeds above Mach 8 at altitudes between 30 km and 38 km for more than 60 s. The nose and forebody section of the payload was made of CMC structures. Three canards with a CMC thermal protection were equipped with thermal management experiments to verify the thermal efficiency of these methods. All engineering science experiments like aerothermal heating of the nose and forebody, CMC material response at temperatures above 2200 K, hypersonic thermal management, shock wave boundary layer interaction, CFRP module with cork coating for high temperature applications, high temperature fin leading edge and radiometer sensors provided unique flight data. A reduced in-flight 3 DoF trajectory simulation running on the flight computer determined the ignition time of the third stage which allowed improved experiment conditions in terms of Mach number and apogee altitude even in the presence of external perturbations.

1. Introduction

Simulation based design of flight hardware is one of the cornerstones of DLR's research programs. It requires high quality validation data, which is representative for the real flight environment. Since ground testing facilities have limitations to duplicate the flight environment, availability of flight data is essential. But, in case of spacecraft development this task is very challenging, since the number of flight experiments and availability of the flight data are very limited. This requires a complementary validation approach using ground and flight testing for gathering reliable data and validation of numerical tools. Numerical tools still have shortcomings in modelling high temperature gas phenomena and gas-surface interaction in such environments [1,2]. This again requires material characteristics to be available for a very broad temperature range. Therefore, ground characterization and qualification of hot structures have to be carried out using modern diagnostic methods. Since ground experiments cannot duplicate the flight environment completely, performing successful flight experiments to achieve the aforementioned goal is essential.

The success of SpaceX's space transportation approach triggered a worldwide uptick in reusable launcher activities. Multiple reuses of the most expensive first stage is the focus of most concepts. Recent system studies [3] show that reusability becomes feasible if the separation of the first stage takes place at Mach numbers between 9 and 12. Simulation of this flight environment in ground facilities is limited and requires further data of flight experiments. Hypersonic flight experiments by means of multi stage sounding rocket configurations are the most cost-efficient options to gather valuable flight data. Using available two stage sounding rocket configurations consisting of S31/S30 stages the achievable Mach number for a payload mass of approximately 300 kg is mostly limited to around 6 [2]. SHEFEX-II flight experiment could reach Mach numbers up to 10 using a much powerful motor combination of S40 and S44 [4], which are currently not available. This limitation in combination with the target payload mass forced the DLR's flight experiment REFEX to focus in guidance and navigation during return flight at Mach numbers from 5 down to subsonic speeds [5]. Therefore, aerothermal loads on hot structures are beyond the REFEX project goals.

Past DLR hypersonic flight experiments reached peak Mach numbers of up to 10 [2,4,6], but the test phase with high aerothermal loads was less than 30 s in each instance. The actually achieved high structure temperatures were not close to the upper limit values of hot structures

* Corresponding author.
E-mail address: Ali.Guelhan@dlr.de (A. Gülhan).

https://doi.org/10.1016/j.actaastro.2023.06.034
Received 31 March 2023; Received in revised form 26 May 2023; Accepted 19 June 2023
Available online 28 June 2023

Nomenclature

q	dynamic pressure Pa
T	Temperature K
v	velocity m/s
α	angle of attack °
φ	Clock angle °
β	yaw angle °

Acronyms /Abbreviations

3 DOF	Three Degrees of Freedom
CFD	Computational Fluid Dynamics
C/C–SiC	Carbon Fibre Reinforced Silicon Carbide
CFRP	Carbon Fibre Reinforced Polymer
CIRA86	COSPAR International Reference Atmosphere
CMC	Ceramic Matrix Composite
CoG	Center of Gravity
DAQ	Data Acquisition System
DMARS	Digital Miniature Attitude Reference System
FADS	Flush Air Data Sensing
IMU	Inertial Measurement Unit
IO	Improved Orion
Ma	Mach number
MORABA	Mobile Rocket Base of DLR
Re	Reynolds number
RLV	Reusable Launch Vehicle
SWBLI	Shock Wave Boundary Layer Interaction
TC	Thermocouple
TPS	Thermal Protection System
USSA76	US Standard Atmosphere 1976

and materials. To close this gap and achieve higher Mach numbers the flight experiment STORT (Key Technologies for High Speed Return Flights of Launcher Stages) uses a three-stage sounding rocket configuration. An additional maneuver will keep the third stage of the STORT configuration within a suppressed trajectory with high integral thermal loads.

After the explaining of main objectives of the STORT flight experiment in the next section, the flight configuration with major payloads is described in the second section, which also includes target properties of the flight trajectory. The selected data of the STORT flight experiment will be discussed in the third section. Concluding remarks describe the main achievement and also next steps of the post flight analysis.

2. STORT flight configuration and payloads

The main scientific objective of the STORT flight experiment is gathering data on aerothermal heating and structural response during a hypersonic flight of long duration with high integral heat loads. As shown in Fig. 1 the vehicle consists of three stages: the S31 first stage, the S30 s stage, and the Improved Orion (IO) third stage. The scientific payload is mounted atop the IO motor; there is an active stage separation system between the S30 and IO motor, but no payload separation system.

As shown in Fig. 2 the forebody section of the payload section is made of CMC based high temperature structure [8]. The ogive is divided in the massive ceramic nose and the four downstream segments, that are instrumented with pressure sensors, heat flux gauges and thermocouples. Based on the experience of previous flight experiments SHEFEX-I and SHEFEX-II, a slender forebody followed by a segment with three canards acting as thermal management experiments have been selected as main scientific payloads [2,4,6].

The ceramic shells of the forebody with a thickness between 5.2 mm and 8.6 mm were equipped with different types of sensors to measure the temperature, pressure, and heat flux distribution on the TPS. These

Fig. 1. STORT three-stage flight configuration.

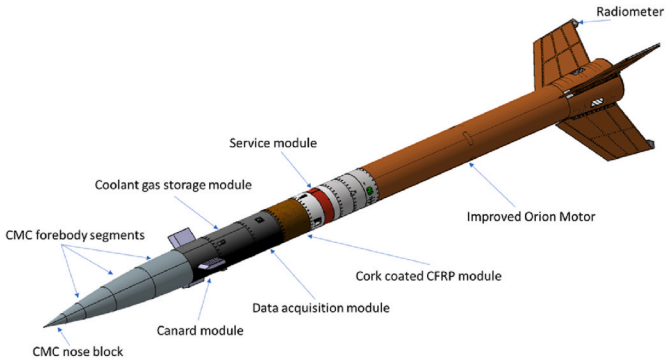

Fig. 2. STORT experiments integrated into the third stage.

shells are mounted to an aluminum substructure via special ceramic supports. Between the ceramic TPS and the substructure, a thick insulation is used for thermal isolation of the payload interior. Special interfaces, mainly for the pressure and heat flux sensors, have been constructed using spring loaded devices to ensure a flush mounting with the TPS panel surface [6,7,9]. To verify the design of these interfaces concerning the temperature resistance of the metallic parts several transient thermal analyses have been performed.

The instrumentation concept of the forebody is derived from previous DLR flight experiments [10,11]. The instrumentation of CMC panels along the lines at 0° and 180° is identical. This is also the case for 90° and 270° lines. For the temperature measurement of the hot structure, different types of thermocouples are used. Kulite pressure transducers of the type XTEH-7L-190 are used for the measurement of the absolute pressure. For the FADS system in the massive C/C–SiC nose, the transducers are mounted to the aluminum structure directly behind the C/C–SiC nose in order to keep the tubing length as short as possible [7,9].

Three canards, which are exposed to severe aerothermal loads during long duration hypersonic flight, have different roles for thermal management experiments. All three canards of the STORT flight configuration have the same interior structural design but different thermal management concepts. The reference canard is made of the standard C/C–SiC material. This canard doesn't have any thermal management, however, the cylindrical canard segment is heavily instrumented to study the Shock-Wave-Boundary-Layer-Interaction (SWBLI) around the canard.

A passive thermal management system in the second canard should keep the leading-edge temperature below a certain level. Due to

previous activities DLR has a certain expertise on passive and active thermal management systems [12,13]. The ceramic material of this canard uses highly conductive carbon fibres with thermal conductivity values of 180 W/(m·K) to enhance passive cooling by means of heat conduction inside the structure.

An active cooling system with monitoring instrumentation is implemented in the third canard. It is known that film cooling or transpiration cooling lead to the contamination of the flow. It changes flow features and makes the interpretation of the flight data difficult. Therefore, the active cooling system of STORT is based on the impingement cooling of the rear surface of the canard leading edge. Multiple injection slots should allow an almost homogenous supersonic impingement of the coolant to the rear inside surface of the C/C–SiC leading edge (Fig. 3) (see Fig. 4).

For in-situ monitoring of potential anomalies of the combustion chamber and nozzle components of the multistage rocket, a radiometer system consisting of three radiometers with different spectral ranges has been developed. It is mounted at the tip of the backside of the Improved Orion stage fin inside a protection housing. To acquire the data of all sensors distributed in different segments of the flight configuration, a special acquisition system (DAQ) is needed. The sensor data of the forebody and three canards is acquired by a data acquisition system which is distributed in three units placed in the DAQ module.

STORT also included the maiden flight of an Inertial Measurement Unit (IMU) developed at MORABA. The IMU features a strapdown design and contains three fiber-optic gyroscopes (FOG) and three quartz servo-accelerometers for measuring angular velocities respectively linear accelerations about the body-fixed axes. Furthermore, the IMU features interfaces for connecting external GNSS receiver as well as an additional high-resolution mode with limited acceleration range that can be used for micro-gravity phases.

The trajectory is designed to feature a low apogee of approximately 45 km and a comparatively far impact ground range of more than 400 km. This requires the use of a low launching elevation angle as well as a coast phase following first stage burnout to allow for the gravity turn to reduce the flight path angle. To achieve a cost-efficient flight experiment, the vehicle concept is based around an inherently safe, passively fin-stabilized sounding rocket design. To reduce the influence of wind and other factors that are difficult or impossible to correct a priori, the third stage ignition time is determined on board based on the actual trajectory rather than the nominal trajectory. The on-board computer ignites the upper stage such that the trajectory deviation with regards to apogee and impact ground range is minimized.

The first stage motor S31 is equipped with 6 fins and has a nominal burning time of 11.5 s. Its passive separation takes place at burnout and leads to approximately 5 km apogee and 6.2 km impact down range. The second stage features a S30 motor with four stabilizing fins and it is ignited 24 s after liftoff; it has a thrust phase of roughly 22 s. At 60 s after liftoff, the third stage separates actively from the second stage at an altitude of 24 km.

The ignition point of the third stage Improve Orion motor is extremely important for the achievement of the mission goals. To ensure that the experiment conditions in terms of Mach number and apogee altitude can be reached even in the presence of perturbations, a dispersion reduction method is employed where the on-board computer chooses the optimum third stage ignition time such that the actual trajectory best matches the nominal trajectory with regards to the apogee altitude and impact ground range. To accomplish this, a reduced 3 DoF trajectory simulation is implemented on the flight computer. The predicted altitude trace of all three stages is shown in Fig. 5.

All these single events yield an expected flight profile in terms of Mach number shown in Fig. 6. According to these predictions the target Mach number of 8 can be reached for a flight period of more than 62 s. The reason of the shorter Mach 8 duration compared to intended 200 s is the mistakenly 10 s delayed ignition of the third stage and achieved lower apogee of 38 km instead of originally planned 47 km. Higher aerodynamic drag force at lower altitude led to stronger deceleration of the vehicle.

Table 1 summarizes the planned main events of the STORT flight experiment.

3. Flight experiment

3.1. STORT assembly and flight trajectory

The assembly of payload segments with a mass of approximately 200 kg and 3.5 m total length was carried out separately from the motor preparation (Fig. 7). Downstream of five CMC segments the canard module with three integrated canards is placed. The outer surfaces of this module, the supply tank segment and the data acquisition module were coated with a zirconia coating for thermal protection. All the modules further downstream featured a cork ablator based thermal protection (Fig. 8).

The main challenge was the integration of the instrumentation into the CMC nose segments and the canard module. Due to limited available space the wire harness situation created some difficulties. Operation of the high-pressure nitrogen supply for the active cooling experiment took longer than planned because of gas leakage at one of the interfaces. A further time-consuming part was the verification of the communication between the service module and telemetry station.

After completion of the assembly and verification of data communication to the data acquisition system and telemetry station, the payload was transferred to the motor launcher assembly block. Fig. 9 shows the main geometrical features of the three stages configuration. The total length of the vehicle is 13.5 m. While the diameter of the first and second stages was 557 mm, the third stage (Improved Orion) and payloads have an external diameter of 357 mm. The total liftoff mass was 3009 kg.

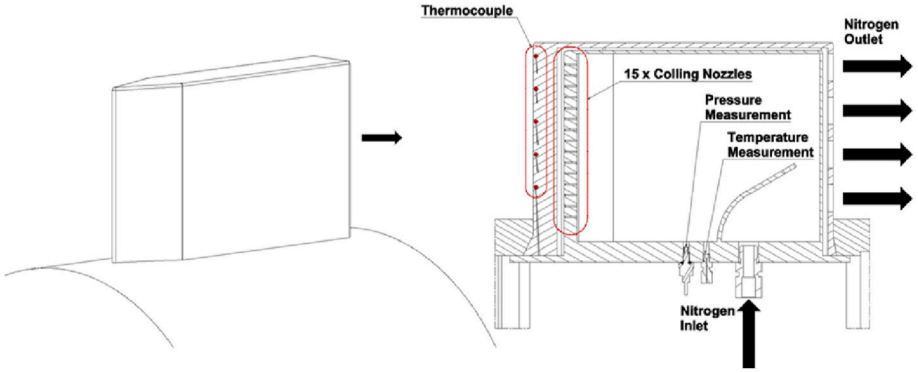

Fig. 3. Canard with impingement cooling.

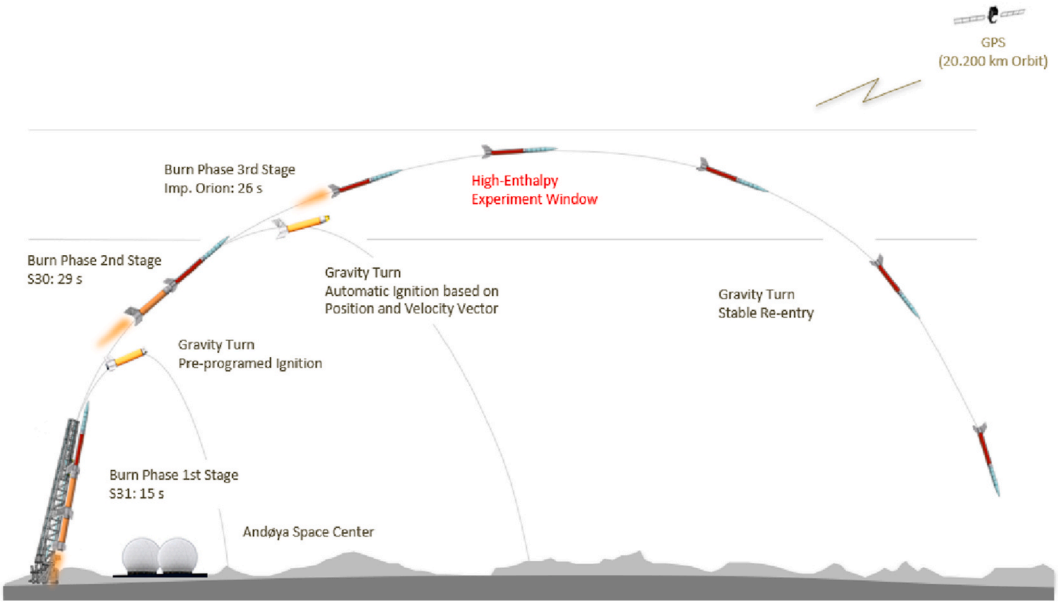

Fig. 4. Main STORT flight phases [14].

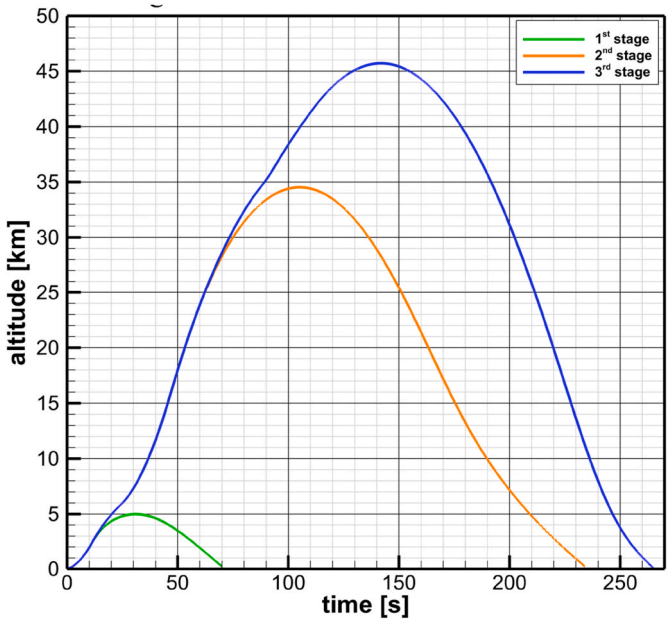

Fig. 5. STORT first, second and third stage altitude over time.

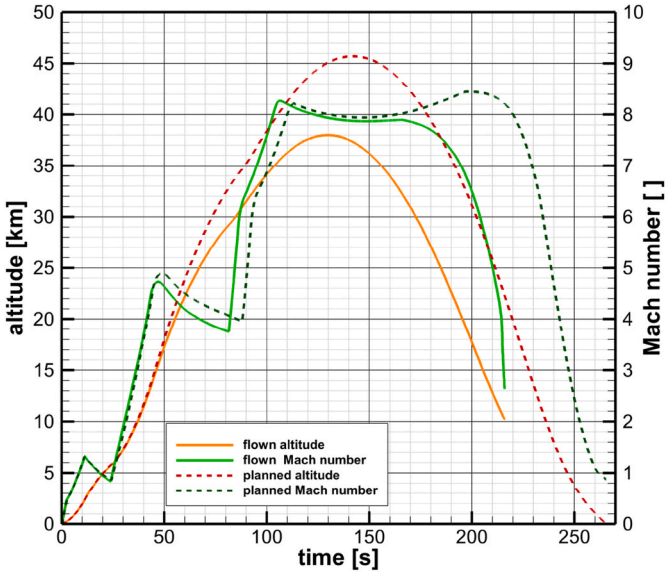

Fig. 6. Planned and flown altitude and Mach number of the STORT third stage and payload.

After several verification tests concerning mechanical and electrical arming and test countdowns, the STORT flight configuration was prepared for the launch at 68° elevation and 330° azimuth (Fig. 10, left). In addition to the wind profile, the state of rain clouds density was one of the key decision criteria for the launch, since signature measurements using a ground base infrared camera system are heavily depending on it. Finally, in the early morning of June 26, 2022, the STORT flight experiment launched on top of the three-stage rocket configuration from the Andøya Space launch site in northern Norway (Fig. 10, right).

3.2. Analysis of results for forebody

As planned the first stage S31 burned out 11.5 s after lift-off and reached a velocity of 429 m/s at an altitude of 2585 m (Fig. 11). Approximately 12.5 s after the passive separation of S31 the second

Table 1
STORT Trajectory key events.

Event	Time [s]	Altitude [km]
S30 Motor Ignition	0.00	0.04
Launch Rail Exit	0.73	0.06
Spin Up Motor Ignition	0.84	0.07
Mach 1	8.39	1.45
S31 Motor Separation (passive)	11.50	2.48
S30 Motor Ignition	24.00	5.80
Maximum Dynamic Pressure	44.30	14.22
S30 Motor Burnout	51.10	18.70
S30 Motor Separation (active)	60.01	23.87
IO Motor Ignition	88.00	34.69
IO Motor Burnout	113.00	42.08
Apogee	141.90	45.73
Impact	265.40	0.00

Fig. 7. Preparation of the STORT payload modules.

Fig. 8. STORT payload modules.

stage S30 was ignited and burned around 21 s. At flight time point of 45.5 s the velocity and altitude were 1384 m/s and 14.5 km, respectively. As mentioned before the ignition time point of the third stage Improved Orion was performed by using actual position and velocity vector data with a 3DoF flight dynamics simulation on-board. The ignition occurred 81 s after the lift-off at an altitude of approximately 29 km.

The third stage with scientific payloads reached a flight speed of 2557 m/s, i.e. Mach number of 8.26 (USSA76 atmospheric model [15]), at an altitude of 36 km and finally reached the apogee of its trajectory at an altitude of 38 km and a velocity of 2497 m/s, which corresponds to a Mach number of 8.0 (Fig. 6). It then descended into the Atlantic Ocean roughly 380 km away from the launch site. During this hot hypersonic flight phase extensive measurement data of the scientific payloads and vehicle was transmitted to the ground station.

Fig. 12 shows the Reynolds number and Mach number map of the flight using two different atmospheric models, i.e. standard US atmosphere model USSA76 and CIRA86 model [16]. The difference between the two models becomes particularly visible at high altitudes. At Mach 5 the unit Reynolds numbers achieved during ascent and descent are 1.95 10^6/m and 2.89 10^7/m, respectively. The unit Reynolds number of 10^7/m is achieved during ascent at a Mach number of 4.4 and an altitude of 29.6 km and during descent at Mach 7.2 and an altitude of 23.2 km. The Reynolds number at the maximum Mach number of 8.26 (USSA76) is $1.3 \bullet 10^6$/m.

The 38 km apogee reached during flight is below the target value of 45.73 km (Table 1 and Fig. 11). The reason for this deviation is a calibration error during the hardware-in-the-loop tests. However, flying at Mach numbers beyond 8 at lower altitudes means higher dynamic pressure and aerothermal loads, thus the STORT payloads were actually exposed to even more severe conditions than anticipated.

The forebody of STORT is an ogive and has a total length of 1500 mm (Fig. 13). As mentioned before the forebody consists of a bulk conical nose with a radius of 2.5 mm and four downstream ogive segments with CMC shell structures as thermal protection. The canard segment of 300 mm length includes three canards, which use again a CMC shell as thermal protection.

Fig. 13 shows the geometry of the forebody, which was heavily instrumented along four rows in 90° circumferential distance from each other. The total length including canard module is 1800 mm.

The CMC nose block was instrumented with one type S thermocouple (TS002V) and two type K thermocouples (TS003V and TS004V) with a diameter of 1 mm and 0.5 mm, respectively. The positions of thermocouples are shown in Fig. 14. Table 2 contains the position of the sensors with reference to the coordinate system defined in Fig. 13. The column with the title “nominal surface distance” includes design values of the position. Due to multiple effects like imperfection in machining of the holes, integration uncertainty, glue effects, etc. The measured distance from the surface is partially remarkably from the design value. For the determination of the exact position of the thermocouple tip inside the CMC structure the Computer Tomography facility at DLR Stuttgart has been used. The values measured there are given in the column “measured surface distance”.

The first CMC shell structure downstream of nose was equipped with type K thermocouples of 0.5 mm in diameter at 45° in circumferential direction below the surface. Pressure ports (PK005V, PK007V, PK009V and PK011V) were mounted at the same axial position as the thermocouples (TK005V, TK013V, TK021V TK021V) but along the different row at 0° in circumferential direction. They were connected to pressure sensors, which were mounted to the metallic substructure of the vehicle.

At sea level before launch all the pressure sensors measure the same pressure of approximately 100 kPa (Fig. 15). A gradual pressure

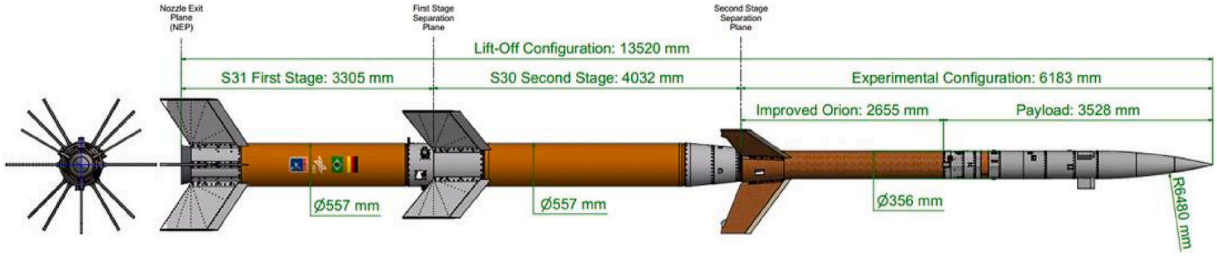

Fig. 9. STORT three stage configuration.

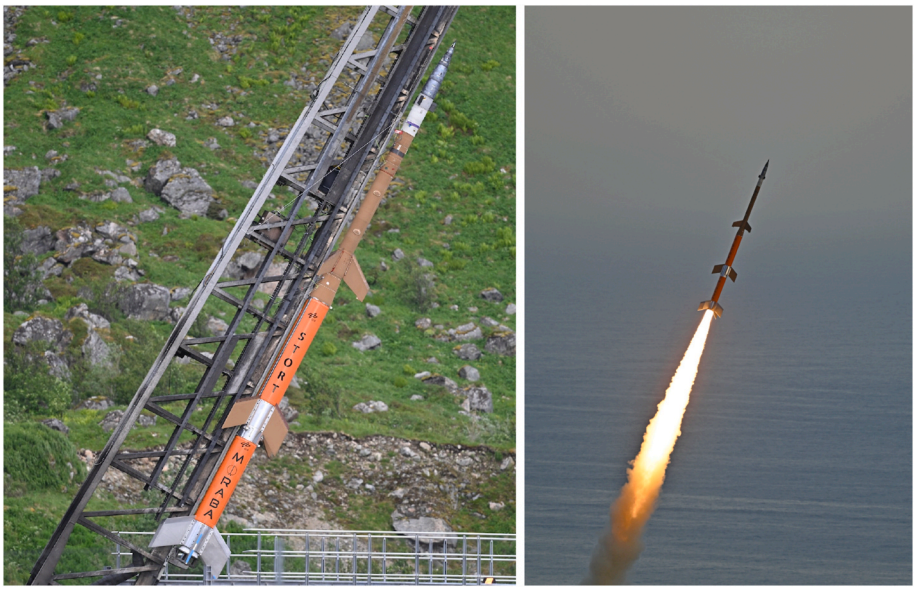

Fig. 10. STORT Flight experiment at the launch pad of Andøya Space Launch Site (left) and launch event (right).

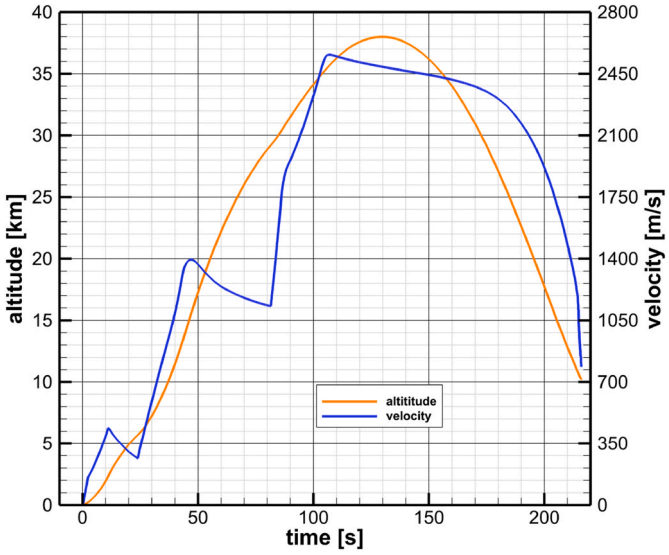

Fig. 11. Altitude and velocity profiles of the STORT flight over the time.

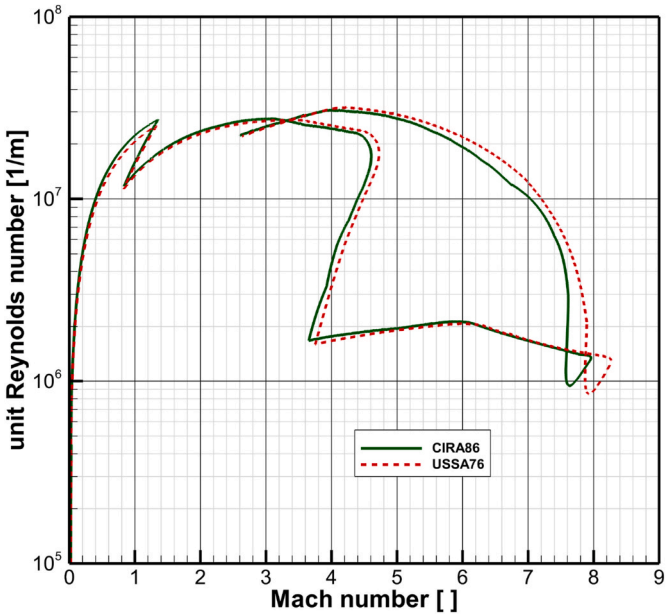

Fig. 12. Mach number vs. unit Reynolds number profile of the STORT flight.

decrease along the axial distance from the nose is visible along the complete flight trajectory. The first small peak around 8.5 s is a result of sonic speed limit passage. The second peak at 24 s after lift-off is caused by the ignition of the second stage S30. The acceleration following the Improved Orion ignition is also clearly visible at around 85 s. The pressure data during descent flight around 180 s after take-off indicates some fluctuations. After this time point the data becomes noisy. A significant peak followed by a data transmission interruption is an indication of a damage to the payload due to significant thermo-mechanical

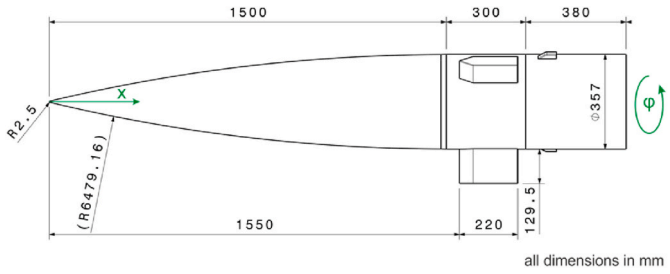

Fig. 13. Geometry of the forebody and canard module.

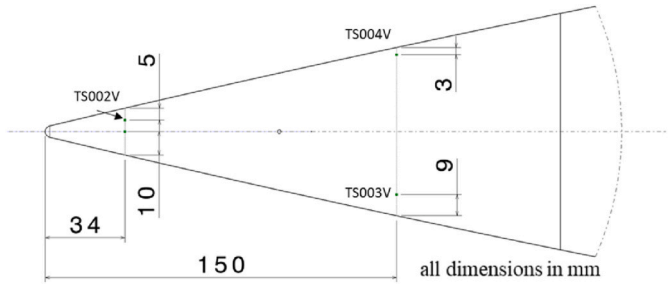

Fig. 14. Thermocouple positions in the nose section.

Table 2
Positions of selected sensors along the forebody.

sensor name	x [mm]	φ [°]	nominal surface distance [mm]	measured surface distance [mm]
TS002V	40	0	5	6,7
TS003V	152,1	315	9	9,3
TS004V	150,5	135	3	2,7
TK001V	230	45	2	4,6
TK005V	300	45	2	5,7
TK009V	410	45	2	2,8
TK013V	550	45	2	3,5
TK017V	710	45	2	2,5
TK021V	800	45	2	3,7
TK025V	1000	45	2	3,3
TK029V	1110	45	2	2,7
TK033V	1200	45	2	3,0
TK037V	1400	45	2	2,9
TK041V	1480	45	2	3,5
PK001V	100	0	port: 0 mm sensor: ~500 mm	
PK005V	300	0	port: 0 mm sensor: 38 mm	
PK007V	550	0	port: 0 mm sensor: 38 mm	
PK009V	800	0	port: 0 mm sensor: 38 mm	
PK013V	1400	0	port: 0 mm sensor: 38 mm	

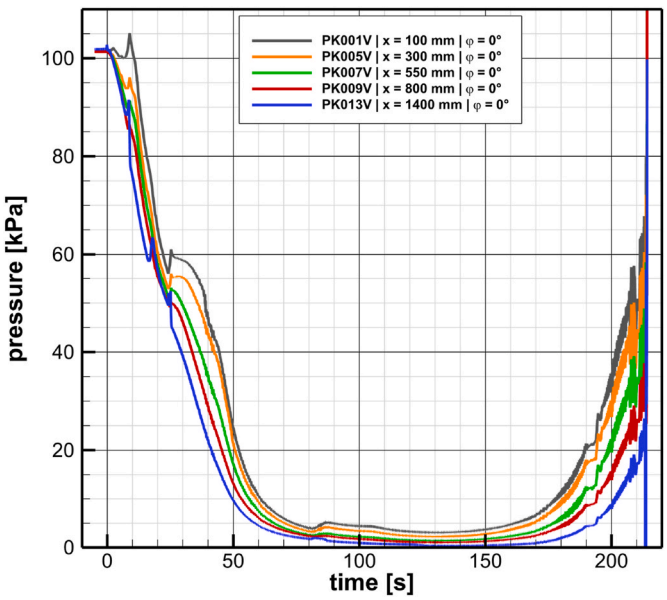

Fig. 15. Measured pressure history along the forebody.

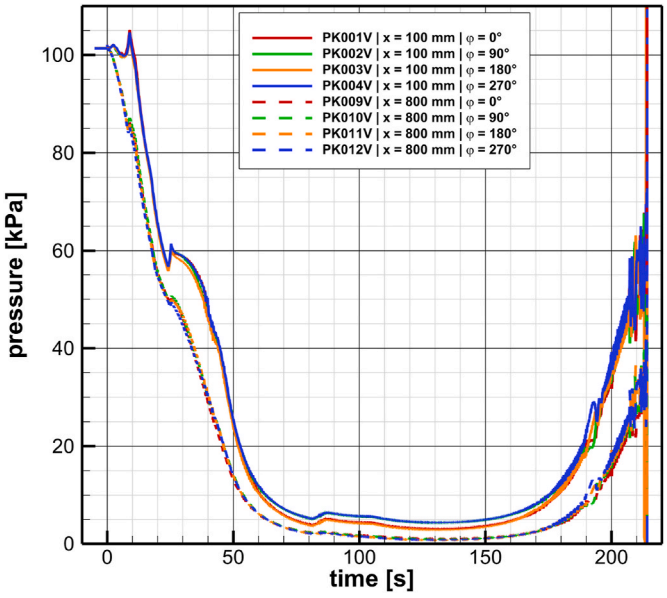

Fig. 16. Measured circumferential pressure distribution at two axial positions from the forebody nose.

loads during low altitude (below 15 km) and high Mach number (above Mach 5) flight. The target valid experimental window was defined for altitudes above 20 km for the descent flight.

In particular pressure sensors of the upstream segments clearly show the ignition of the third stage around 81 s after take-off (Fig. 16). At high altitudes the circumferential pressure distribution at axial position of 100 mm from the nose indicates a small pressure difference between pitch and yaw planes. Since this difference disappears at 800 mm distance to the nose, small local asymmetry in the geometry of the nose segment might be the reason.

Fig. 17 shows measured temperatures inside the CMC nose block. As mentioned before the thermocouple TS002V is a type S thermocouple and positioned in 34 mm axial distance from the nose tip (Fig. 14). It is mounted to the block 5 mm beneath the surface. Measured temperature history correlates nicely with the motor ignition and separation times as shown in Figs. 11 and 6. The maximum temperature of 1382 K is reached at the flight time point of 208 s, which corresponds to a Mach number of 5.3 at 13.8 km altitude during descent flight. The other two type K thermocouples are positioned 150 mm downstream of the nose tip (see Table 2) but are in different distances to the surface (Fig. 14). Thermocouple TS004V is closer to the surface (3 mm in contrast to 9 mm distance of TS003V) and measures higher temperatures. It shows also a faster response to the increase of aerothermal loads at the flight time point around 190–200 s. An increase of the temperature followed by a sudden decrease at this flight time point will be discussed later.

Fig. 18 shows measured CMC structure temperature evolution along the row at 45° in circumferential direction. For a better visualization solid lines are used for upstream thermocouples while dash dot curves belong to the downstream thermocouples. All thermocouples are

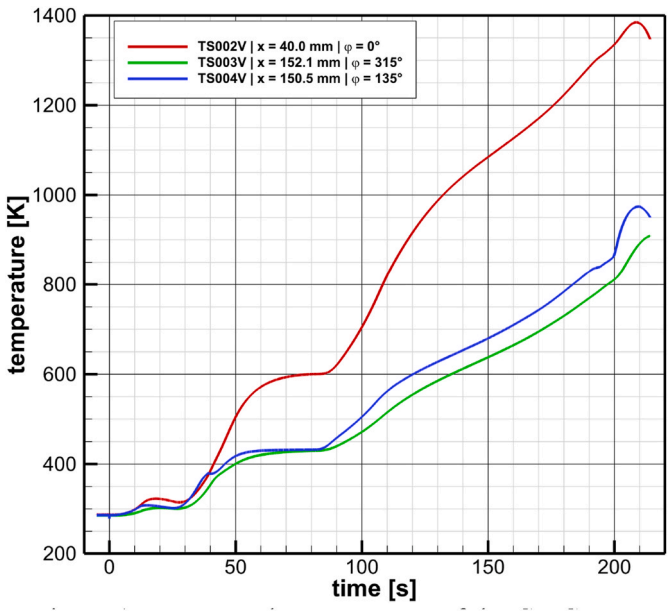

Fig. 17. Measured temperatures of the CMC nose block.

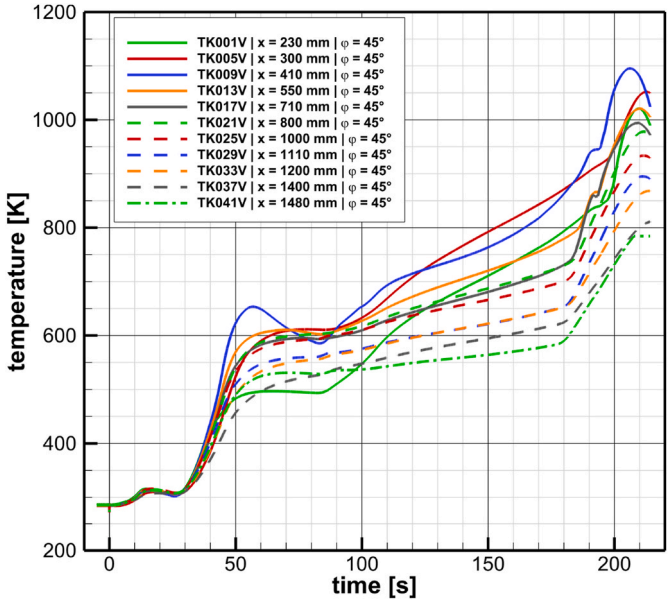

Fig. 18. Measured temperature forebody temperature evolution along the 45° row of the forebody.

integrated at approximately 2 mm beneath the surface of the CMC shells. It is well known that even slight differences in integration process can have a remarkable effect onto the response time of thermocouples [6]. Therefore, measured gradients after the ignition of the second stage S30 partially deviates from each other. In the flight phase at Mach numbers above 6 (after 85 s) the nose becomes hot and clear differences in thermocouple data are visible. TK001V is placed very close to the interface between the nose block and the first CMC shell (Table 2). Due to the graphite-based gap filler this point has a good thermal conduction to the massive nose block. The temperature of the massive CMC block at the interface at flight time point of 40 s is below 350 K (Fig. 17). At the same time TK001V measures 450 K. That means heat conduction from the CMC shell to the upstream CMC nose block, which should lead to a temperature decrease at the location of TK001V. But, at the same time the velocity and convective heating increases due to the thrust phase of the S30 motor. The combination of these two physical processes ends at an almost constant temperature history until the ignition of the third stage at 80 s. The temperature gradient decrease at 45 s correlates with the temperature profile measured with the TS004V thermocouple, which is very close to the cone surface and therefore shows a fast response to changes of aerothermal loads. It is also in good agreement with decreasing thrust of the S30 motor, which is clearly visible in the longitudinal acceleration (Fig. 22).

After 80 s the profile measured with TK001V is similar to that of TK009V, which is positioned at the interface between second and third CMC shells. The reason of the lower temperature level at the more upstream TK001V position could be a heat sink effect of the cooler massive nose due to its high heat capacity or imperfect contact between the thermocouple and CMC material. Since the temperature increase due to laminar turbulent boundary layer transition around 180–200 s during descent flight is captured correctly, the second hypothesis was less plausible. But the final answer can only be given with a dedicated ground test or coupled simulation of the flight. TK041V thermocouple measures the temperature increase due to boundary layer transition first and the most upstream thermocouple last. This demonstrates nicely that laminar turbulent transition starts downstream and moves upstream over time. The temperature decrease measured with TK009V during the non-thrust ascent flight phase is probably linked to the turbulent to laminar boundary layer transition during ascent (Fig. 18). Corresponding Mach number and unit Reynolds number in this flight period are approximately 4.6 and 13.0 $\times$ 10^6/m, respectively. The unit Reynolds number is in the order of values of laminar to turbulent transition points of the ROTEX-T flight experiment [17]. ROTEX-T forebody was made of a smoot stainless steel cone with a half angle of 7° and its surface temperature was remarkably lower than the temperature of the CMC forebody shells of STORT. A further difference is the different thermal mass of each segments of STORT resulting from massive nose block and higher thermal conductivity at interfaces to the substructure. This effect together with the low response time of thermocouples smear the temperature profile caused by the boundary layer transition process.

During descent flight the Mach number at 180 s is 7.7 at an altitude of 26.6 km. This corresponds to a unit Reynolds number of 4.5 $\times$ 10^6/m. This Reynolds number level is also in the range of transition Reynolds numbers measured during previous flight experiments [17,18]. The weak or moderate response of all other sensors cannot be answered without further detailed analysis.

Thermocouples TK005V, TK013V, TK021V, TK025V, TK033V and TK037V are far from the nose integrated in the middle part of each CMC shell segment and have a good thermal isolation to the Aluminum substructure and are placed far from the four stand-offs, which could augment heat conduction from the TPS panel to the sub-structure. Therefore, compared to other thermocouples close to the interfaces with potential step-up gap or step-down effects the temperature response of those thermocouples mainly depends on convective heating and thermocouple response time. Nevertheless, only thermocouples TK013V, TK017V and TK009V measure a slope change around 190 s. Whether this behavior is linked to some potential changes on the surface of the second segment cannot be answered with the available information level at this moment. This point also requires further investigations.

3.3. Analysis of results for canard module

As mentioned before three CMC canards were designed for different type of experiments. The segment portion around the reference canard without cooling was instrumented with multiple high response instrumentation and data acquisition to measure the shock wave boundary layer interaction effects along the complete supersonic/hypersonic flight trajectory regime. The outer shell of the canard is made of CMC structure, which is protecting the interior Titanium structure. Fig. 19 shows measured temperature history at distinct points of the CMC leading edge. Five type K thermocouples were integrated 2 mm beneath

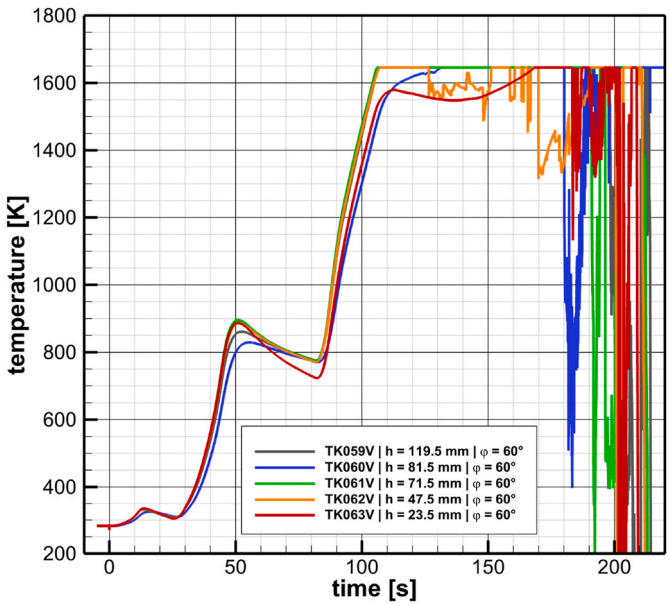

Fig. 19. Measured temperature history of the reference canard leading edge.

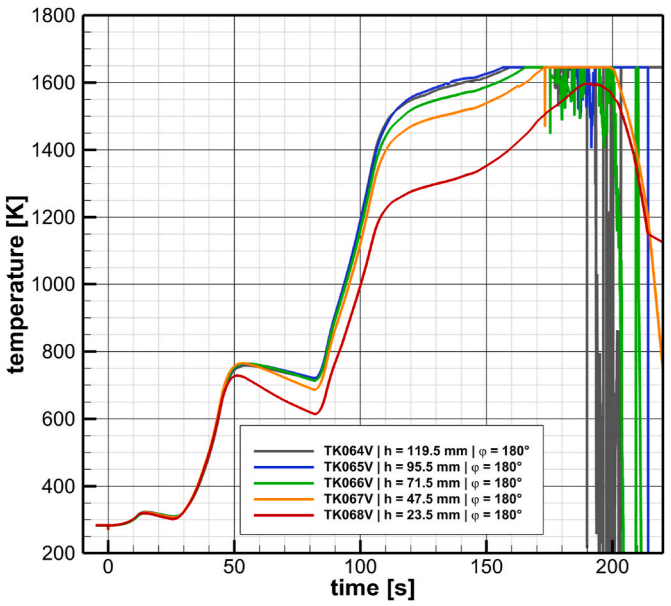

Fig. 20. Measured temperature history of the canard leading edge with passive thermal management.

the leading surface at radial distances of 50 mm, 74 mm, 98 mm, 108 mm and 146 mm from the base of the CMC canard shell. The difference in measured temperature gradients during burning phase of the S30 motor (between 24 s and 51 s) is mainly linked to different response times, which strongly depends on the quality of the thermocouple contact to the structure and its exact position. Thermocouples TK063V, TK062V and TK061V have the best response times and reach the same maximum temperature of 900 K in the S30 thrust phase. In the no-thrust phase immediately after S30 burn-out TK063V measures strongest temperature decrease. Since it is the sensor closest to the canard segment, the heat conduction from the canard to the cylindrical body is higher compared to other thermocouple points. Furthermore, the lower part of the canard is exposed to the boundary layer flow with lower aerothermal heating, which means lower surface temperature in this area.

The same thermocouple (TK063V) measures the lowest temperature in the burning phase of the third stage motor (Improved Orion). All other type-K thermocouples reach the operation limit temperature of 1650 K before 130 s flight time. Only TK063V is still operational until 170 s. After the burn-out of the Improved Orion motor at around 113 s TK063V measures decreasing temperatures, which is as expected. During descent phase after achieving the apogee around 124 s (see Table 1) the heat flux rate and the surface temperature increase again. Finally, at 170 s the limit temperature is reached and the signal is saturated. Because of increasing heat fluxes surface temperatures increase further and all thermocouples lose their functionality.

The Shock Wave Boundary Layer Experiment (SWBLI) was one of the key aerothermal experiments of the STORT flight experiment [19]. Heat flux and pressure sensors with a fast response time mounted around the canard measured the foot print of the shock wave boundary layer interaction on the canard module surface. The instrumentation design of this payload is carried out in cooperation with the University of Arizona using experimental and numerical tools. Post flight data processing of this experiment is still ongoing.

The second canard was devoted to the passive cooling experiment. High thermal conductive fibers are used to increase the thermal conductivity of the CMC material. It results in a better heat dissipation inside the structure and higher heat conduction to the interfaces. Fig. 20 includes measured temperature evolution at points with the same radial distance to the canard module surface as in case of reference canard. Measured gradients of all five thermocouples from lift-off up to the burn-out of the second stage motor are very similar. The maximum temperature of 750 K compared to 900 K of the reference canard at the same time point is significantly lower. Thermocouples TK064V and TK065V with the maximum distance to the module interface measure the highest temperature. TK068V with the smallest distance measures again the lowest temperature. The gradient during no-thrust phase after S30 burn-out is more distinct than in the reference case. This thermocouple operated throughout the complete flight and measured a maximum temperature of 1600 K during descent at 190 s after lift-off. All other thermocouples provide data until much later into the descent flight phases. This data demonstrates clearly the success of the passive cooling concept of STORT. Together with the reference canard flight data it provides a unique data base for validation of numerical simulations and physical understanding of hypersonic flight physics.

The active thermal management experiment on the third canard was based on the impingement cooling. Three high pressure nitrogen bottles with a pressure of 250 bars and a volume 6 L were installed into the so-called coolant gas storage module (Fig. 2). The required nitrogen mass flow rate was determined using simplified analytical predictions. Coolant gas nitrogen is accelerated to the rear surface of the leading edge using multiple supersonic nozzles. The mass flow rate is controlled by means of a pressure regulation valve. The flight readiness of this payload in Andøya took a long time because of gas leakage at one of the interfaces. The problem was fixed before the flight. But, the post flight data showed very low measured coolant mass flow rate, which was unfortunately not sufficient to perform impingement cooling. Therefore, this data can be used as cross-check of the reference canard flight data. In this case all five thermocouples (TK069V, TK070V, TK071V, TK072V and TK073V) measure very comparable temperature gradients from lift-off up to achieving the thermocouple limit temperature of 1650 K (Fig. 21). The maximum temperature achieved at S30 burn-out point is the same as in case of the reference canard with 900 K. It seems here similarity of thermocouple contacts and their positions inside the structure are much better. Similar to the thermocouple TK063V of the reference canard, TK073V measures the lowest temperature and is operational until approximately 170 s. This data indicates a good symmetry of the flow around the payload, which means a flight at low angle of attack and yaw angle. This point is discussed below.

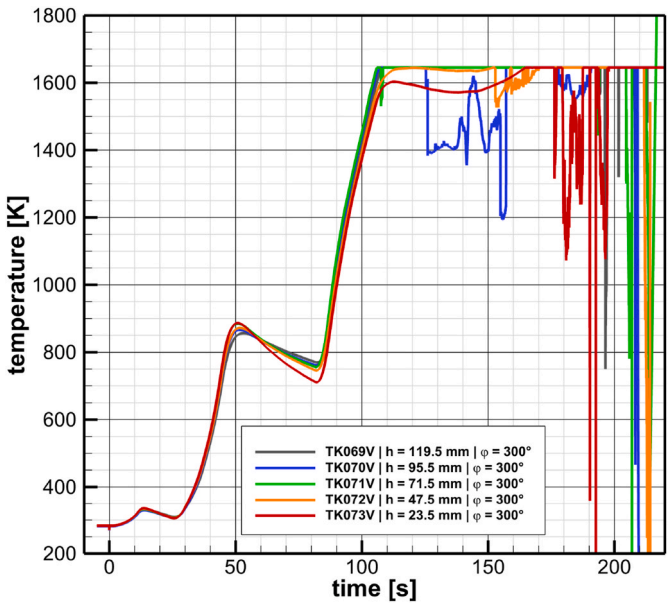

Fig. 21. Measured temperature history of the canard leading edge with active cooling.

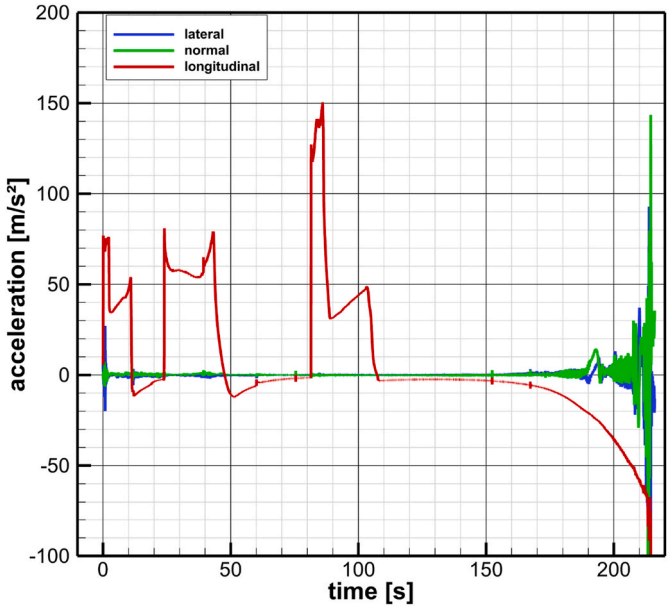

Fig. 22. Measured accelerations during STORT flight.

3.4. Analysis of mission data

The acceleration data of the DMARS system confirm measured aerothermal response of structures but brings some complexity into the interpretation (Fig. 22). Longitudinal acceleration data follows expected ignition, thrust and burn-out phases of all three stages perfectly. At around 155 s after lift-off the axial deceleration of the vehicle increases. At this point the Mach number is around 8 at an altitude of 31 km. But, at the same time in both lateral and normal directions a short acceleration peak followed by an oscillatory behavior around the zero-g line is visible. At around 210 s these oscillations are enhanced and lead to strong acceleration peaks in all three directions. It corresponds to the flight trajectory point with a Mach number of 4.9 at 13 km altitude. A detailed analysis of the anomaly is still ongoing.

Similar to the most of sounding flight experiments STORT vehicle was also because of missing thrust vector control system spin stabilized. Compared to the fins of S30 and IO motors six fins of the first stage S31 were deflected slightly more to initiate the spin of all three stages including payloads at low speeds. This effect is also visible in sharp gradients during engine-on and stage separation events (Fig. 23). Due to separation relation between the fin surfaces and roll inertia moment changes and leads to a change in vehicle spin behavior. The four fins of S30 and three fins of IO had also a small deflection angle to induce spin, which increases in the thrust phase due to axial acceleration. Measured roll angular rate history shows an interesting behavior. An increase of the roll rate during active thrust phases is followed by a slight decrease for the timeslots without thrust. The burn-out time point of 11.5 s and 45 s of both S31 and S30 motors correlates to the roll rate decrease points. Separation of the S30 motor in the no thrust phase around 60 s also causes a roll rate increase, which is followed by a decrease until the ignition of the IO motor at the time point of 81 s. The high thrust phase of 4 s leads to a further increase of the roll rate, which changes its slope during the sustain phase of IO motor. At the burn-out point of IO motor around 113 s a rate of 870°/s is reached. Until the apogee point of 132 s the roll rate remains around 900°/s and starts to decrease during descent flight due to aerodynamic damping effects.

For in-situ monitoring of potential anomalies of the combustion chamber and nozzle components a radiometer system consisting of three radiometers with different spectral ranges has been developed. It is mounted to the tip of the backside of the rear fin inside a protection housing. Post flight data processing of this experiment is challenging and still ongoing.

4. Concluding remarks

The long duration hypersonic experiment STORT with more than 60 s Mach 8 flight at an altitude between 30 km and 38 km has been carried out successfully using a three-stage sounding rocket configuration. The instrumentation of the main scientific payloads like the forebody, three fixed canards, thermal management experiments and shock wave boundary layer interaction experiment delivered unique data of a hypersonic flight. Three radiometers mounted to the rear part of the third stage fins measured plume radiation in different spectral ranges. A reduced in-flight 3 DoF trajectory simulation implemented on the flight computer allowed to achieve experiment conditions in terms of Mach number and apogee altitude by means of an on-board selected optimum third stage ignition time point. A new Inertial Measurement Unit (IMU) developed at DLR has been flight qualified.

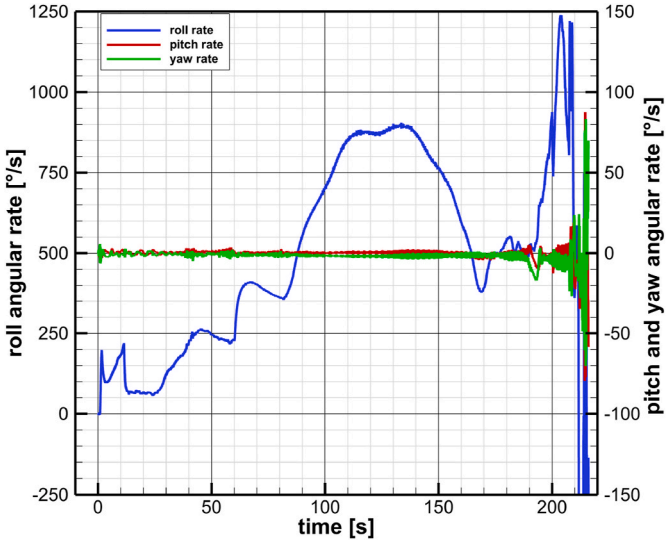

Fig. 23. Measured angular rates during STORT flight.

The STORT flight had a hypersonic flight phase at Mach numbers between 5.0 and 8.2 with a duration of 126 s. The duration of a flight phase above Mach 8 at altitudes between 30 km and 38 km was 62 s. The apogee of 38 km was lower than the target value of 45.7 km, which led to higher aerothermal loads, since the Mach number range was comparable to the planned values.

The STORT flight provided unique data on aerothermal heating and response of the CMC structures during a long duration hypersonic flight. The impact of motor ignition and thrust driven phases on surface temperature evolution could be measured clearly. Although complex heat dissipation phenomena inside the structure partially influence the measurements and the heat flux also changes due to boundary layer transition, thermocouple data of the forebody clearly show these effects during ascent and descent flight. Passive thermal management using high conductive fibers for the CMC canard structure demonstrated its high potential for future applications. Due to gas leakage problems of the impingement cooling experiment the performance of this technique during flight could not be demonstrated. However, a remarkable experience has been gained with respect to its future flight implementation. The detailed post flight analysis of the flight data is in progress and will be completed in the coming few months. This is true especially for those experiments that need careful analysis and interpretation, such as the radiometer, boundary layer transition and shock-wave boundary layer interaction experiments.

Declaration of competing interest

We wish to draw the attention of the Editor to the following facts which may be considered as potential conflicts of interest and to significant financial contributions to this work.

We wish to confirm that there are no known conflicts of interest associated with this publication and there has been no significant financial support for this work that could have influenced its outcome. We confirm that the manuscript has been read and approved by all named authors and that there are no other persons who satisfied the criteria for authorship but are not listed.

We further confirm that the order of authors listed in the manuscript has been approved by all of us. We confirm that we have given due consideration to the protection of intellectual property associated with this work and that there are no impediments to publication, including the timing of publication, with respect to intellectual property.

In so doing we confirm that we have followed the regulations of our institutions concerning intellectual property. We further confirm that any aspect of the work covered in this manuscript that has involved either experimental animals or human patients has been conducted with the ethical approval of all relevant bodies and that such approvals are acknowledged within the manuscript.

We understand that the Corresponding Author is the sole contact for the Editorial process (including Editorial Manager and direct communications with the office). He/she is responsible for communicating with the other authors about progress, submissions of revisions and final approval of proofs.

Acknowledgment

The research project STORT including the flight experiment was funded by the DLR's Program Directorate for Space Research and Development.

References

[1] A. Mack, R. Schäfer, A. Gülhan, B. Esser, IMENS flowfield topology changes due to fluid-structure interaction in hypersonic flow using ANSYS and TAU, in: C. Breitsamer, B. Laschka, H.J. Heinemann, R. Hilbig (Eds.), New Results in Numerical and Experimental Fluid Mechanics IV, Springer, 2004, pp. 196–203.

[2] T. Barth, Aero- and thermodynamic analysis of SHEFEX-I, Engineering Applications of Computational Fluid Mechanics 2 (No. 1) (2008) 76–84.

[3] L. Bussler, S. Stappert, J. Wilken, M. Sippel, I. Dietlein, S. Karl, C. Hantz, „Analysis of VTVL and VTHL reusable launch vehicle configurations", in: 1st FAR Conference, Monopoli, Italy, 2019. September 30th – October 3rd, https://elib.dlr.de/135448/.

[4] H. Weihs, J. Longo, A. Gülhan, Sharp Edge Flight Experiment SHEFEX," Fourth European Workshop on Thermal Protection Systems and Hot Structures Conference Proceedings, ESA SP-521, Noordwijk, The Netherlands, 2002.

[5] Peter Rickmers, Waldemar Bauer, Wübbels Guido, Sebastian Kottmeier, Refex: reusability flight experiment - a project overview, in: 8th European Conference for Aeronautics and Space Sciences, EUCASS), 2019.

[6] Ali Gülhan, Dominik Neeb, Thomas Thiele and Frank Siebe; Aerothermal postflight analysis of the sharp edge flight experiment-II . J. Spacecraft Rockets, DOI: 10.2514/1.A33275. ISSN 0022-4650.

[7] T. Thiele, D. Neeb, A. Gülhan, Post-flight hypersonic ground experiments and FADS flight data evaluation for the SHEFEX-II configuration, in: Proceedings of 8th European Symposium on Aerothermodynamics for Space Vehicles, ESA, March 2015.

[8] Giuseppe D. di Martino, Thomas Reimer, Lucas Dauth, Luis Baier, Structure Design of a Sounding Rocket Forebody with a Segmented Filament Winding-Ceramic Matrix Composite Thermal Protection System, HiSST, 2nd International Conference on High-Speed Vehicle Science technology, Bruges, Belgium, September 2022, pp. 11–15.

[9] Gülhan, Ali und Thiele, Thomas und Siebe, Frank und Kronen, Rolf und Schleutker, Thorn (2018) Aerothermal Measurements from the ExoMars Schiaparelli Capsule Entry . Journal of Spacecraft and Rockets. American Institute of Aeronautics and Astronautics (AIAA) DOI: 10.2514/1.A34228 ISSN 0022-4650.

[10] T. Thiele, A. Gülhan, H. Olivier, Instrumentation and aerothermal postflight analysis of the rocket technology flight experiment ROTEX-T, J. Spacecraft Rockets 55 (No. 5) (September–October 2018).

[11] A. Gülhan, F. Klingenberg, F. Siebe, A. Kallenbach, I. Petkov, Main Achievements of the Sounding Rocket Flight Experiment ATEK, IAC, Dubai, October , x62713. IAC-21,D2,6,4.

[12] B. Esser, et al., Innovative thermal management concepts and material solutions for future space vehicles, J. Spacecraft Rockets 53 (6) (2016) 1051–1060, https://doi.org/10.2514/1.A33501.

[13] H. Böhrk, M. Kuhn, H. Weihs, Concept of the heat balance of the transpiration-cooled heat shield experiment AKTIV on SHEFEX II, in: Proceedings of the 6th European Workshop on Thermal Protection System and Hot Structures, European Space Agency, Noordwijk, The Netherlands, April 2009.

[14] A. Gülhan, D. Hargarten, M. Zurkaulen, F. Klingenberg, F. Siebe, G. di Martino, T. Reimer, Objectives and Achievements of the Hypersonic Flight Experiment STORT, IAC-22, Paris, September 2022, pp. 18–22. IAC-22, D2,6,7,x69473.

[15] National Oceanic and Atmospheric Administration, National Aeronautics and Space Administration, and United States Airforce, U.S. Standard Atmosphere, U.S. Government Printing O-ce, Washington D.C., 1976, 1976. url, https://ntrs.nasa.ov/api/citations/19770009539/downloads/19770009539.pdf.

[16] D.E. Rees, J.J. Barnett, K.B. Labitzke, "COSPAR international reference atmosphere, Pt. 2: Middle atmosphere models", Advances in Space Research 10 (12) (1986), 1990.

[17] Thomas Thiele, Gülhan Ali, Herbert Olivier, Instrumentation and aerothermal post-flight analysis of the rocket technology flight experiment ROTEX-T, in: Journal of Spacecraft and Rockets, American Institute of Aeronautics and Astronautics, 2018. AIAA). ISSN 0022-4650.

[18] T.J. Juliano, J. Poggie, K.M. Porter, R.L. Kimmel, J.S. Jewell, D.W. Adamczak, "HIFIRE-5b heat flux and boundary-layer transition", J. Spacecraft Rockets 55 (6) (2018) 1315–1328, https://doi.org/10.2514/1.A34162.

[19] A. Gülhan, S. Willems, F. Klingenberg, D. Hargarten, M. Hörshgen-Eggers, Sport Flight Experiment for High Speed Technology Demonstration, Dubai, October 25-29, 2021. IAC-21,D2,6,5,x62714.